Identification of the neutral carbon ⟨100⟩-split interstitial in diamond

D. C. Hunt, D. J. Twitchen, M. E. Newton,* and J. M. Baker
Department of Physics, University of Oxford, Clarendon Laboratory, Parks Road, Oxford OX1 3PU, United Kingdom

T. R. Anthony
General Electric Company, Corporate Research and Development, Building K1, Room IC30, Schenectady, New York 12301

W. F. Banholzer
General Electric Lighting, 1975 Noble Road, Nela Park, Cleveland, Ohio 44112-6300

S. S. Vagarali
GE Superabrasives, 6325 Huntley Road, Worthington, Ohio 43085
(Received 6 May 1999; revised manuscript received 11 August 1999)

A systematic study has been made of some of the properties of R2, the most dominant paramagnetic defect produced in type-IIa diamond by electron irradiation. R2 has been produced in high-purity synthetic diamonds, which have been irradiated with 2 MeV electrons in a specially developed dewar, allowing irradiation down to a measured sample temperature of 100 K, at doses of 2×10^{17} to 4×10^{18} electrons cm^{-2}. The production rate of vacancies [1.53(10) cm^{-1}] was the same for irradiation at 100 K as at 350 K, but the production rate of the R2 electron-paramagnetic-resonance (EPR) center is 1.1(1) cm^{-1} at 100 K and only 0.10(5) cm^{-1} at 350 K. Measurements have been made of the angular variation of the EPR linewidth, ^{13}C hyperfine structure of samples grown with enriched isotopic abundance of ^{13}C, and of the EPR of samples annealed under uniaxial stress (for which a special equipment was developed). A combination of these data with the previously measured data has shown that R2 is the neutral ⟨100⟩-split self-interstitial. This is an identification of an isolated stable self-interstitial in a group IV material. This shows that the self-interstitial is not mobile in type-IIa diamond under normal conditions (i.e., without the irradiation) until the annealing temperature of 700 K.

I. INTRODUCTION

In recent years there has been a resurgence of interest in radiation-induced defects in diamond (see, for example, Refs. 1–3). The reasons for this interest are at least threefold: first, the availability of high-quality synthetic diamonds enriched with ^{13}C has created the opportunity to determine the structures of intrinsic irradiation damage defects using hyperfine structure in electron paramagnetic resonance (EPR);[3] second, it has been proposed that diamond would make an ideal material from which to build particle detectors (see, for example, Refs. 4 and 5); and third, exploitation of ion implantation techniques to dope diamond requires an understanding of the defects produced during implantation.[6] In view of this, the understanding of irradiation damage defects is vital for full exploitation of the properties of this material.

During irradiation of a crystalline solid such as diamond by energetic particles (electrons, neutrons, etc.) the particle-atom collisions can transfer sufficient energy to the atoms of the solid to cause them to be displaced from their crystal-lattice sites. This results in the production of lattice defects, of which the simplest form are interstitials and vacancies. The vacancy has been well studied both in its neutral (V^0) and negative (V^-) charge states by optical spectroscopy and EPR,[7,8] but the isolated interstitial has not previously been identified. It was predicted theoretically that the most likely state of the interstitial would be the ⟨100⟩-split interstitial,[9,10] which we shall label $\mathbf{I}^0$. The EPR center R1 has been identified as a pair of nearest neighboring ⟨100⟩-split interstitials $[\mathbf{I}-\mathbf{I}]^0$.[3]

The R2 EPR center[11] and the vacancy are always the dominant defects created in extrinsic defect free diamond (labeled *type* IIa) on room-temperature irradiation with 2 MeV electrons. The R2 EPR defect is also formed by neutron and gamma irradiation. We have studied R2 in an attempt to characterize this defect, the structure of which has been a mystery for nearly 40 years.

In this paper we present new work on the R2 EPR defect, which, together with old evidence, shows that R2 corresponds to the neutral ⟨100⟩-split self-interstitial, and that, at least in its uncharged state, the interstitial is immobile up to near its annealing temperature of 700 K.

The paper is organized as follows. Previous work on electron irradiation damage, and the R2 defect, is reviewed in Sec. II, the experimental details are discussed in Sec. III, and the results are presented in Sec. IV. Then Sec. V shows how the data, taken together with previous data, leads to the conclusion about the molecular model of the R2 defect described in Sec. VI.

II. PREVIOUS WORK

A. Previous information about the vacancy in diamond

As the vacancy is relevant to our discussion, its properties will be briefly reviewed. It is the most abundant species of defect produced by electron or neutron irradiation. In the neutral and negatively charged state, it retains its tetrahedral symmetry, but it may undergo a Jahn-Teller distortion to C_{2v}

symmetry in the positively charged state, although this has never been conclusively observed.

The ground state of the neutral vacancy is ^1E, which is not EPR active, and no EPR has been observed which could be attributable to a nearby spin triplet state. Therefore any $S=1$ state is presumed to lie more than 200 meV above the ground state, so that it is insufficiently populated at 300 K.

A broad absorption spectrum is observed in the visible region, with strong zero-phonon lines (ZPL's), labeled GR1, at 1673 meV, with a weaker component at 1665 meV.[7] These lines correspond to transitions between the ground ^1E, and low-lying $^1A_1$ states to the $^1T_2$ state of V^0. The intensity of the line at 1673 meV may be used to calibrate the concentration of V^0 in the sample: the proportionality constant between the integrated ZPL absorption and its concentration has recently been redetermined.[12] A strong influence on the relative concentration of V^-/V^0 is the concentration of substitutional donor nitrogen atom impurities (N_s^0).

Some early work[13] showed that in natural type-IIa diamonds, after neutron or gamma irradiation, the GR1 zero-phonon line (and associated GR2-GR8 lines) were broadened and shifted by 14 and 10 meV, respectively, to the high-energy side of the position measured in room-temperature electron irradiated samples. After annealing the neutron or gamma irradiated diamonds to 780 K, the GR1 zero-phonon line sharpened and moved to the position (1673 meV) measured in room-temperature electron irradiated diamonds. In contrast the line at 1859 meV, which has been associated with the R2 EPR center,[14] was only shifted by 4 meV (similar to the uncertainty of the measurement).

The effect of uniaxial stress on GR1 has been measured.[15,16] These stress studies confirmed the T_d symmetry, and the nature of the ground ^1E and excited $^1T_2$ state associated with the 1.673 eV ZPL. The degenerate ^1E ground state suffers a dynamic Jahn-Teller distortion that splits it into an E (ground) and A state (8 meV higher).

In diamond, the annealing behavior of the vacancy is relatively well understood. It is thought that negative vacancy centers (V^-) undergo a reversible charge transfer process to V^0 before they migrate at 900 K,[7] and V^0 migrates with an activation energy of 2.3(3) eV.[7] The loss of vacancies at lower temperatures (700–800 K), when the vacancy is not mobile, is thought to be due to recombination with a mobile self-interstitial; the activation energy for this process was measured to be 1.4 eV,[17] and more recently to be 1.68(15) eV.[18] It is not known whether this energy corresponds to that required to release the self-interstitial, to its migration energy, to a recombination energy, or some combination of these.[19]

B. Previous information about the interstitial

We have already mentioned that theoretical calculations predict the ⟨100⟩-split self-interstitial (sometimes known as the interstitialcy) is expected to be the most stable.[9,10] Figure 1(a) shows the structure of $\mathbf{I}^0$ (D_{2d} symmetry), the two central carbon atoms are sp^2 bonded, each having a nonbonding p_π orbital normal to the plane containing the sp^2 bonds: these p_π orbitals are normal to the [100] direction joining the two carbon atoms, and to one another. Although $\mathbf{I}^0$ may be oriented along any of the ⟨100⟩ directions, we shall occasionally discuss the $\mathbf{I}^0$ oriented along [100] as it will be necessary to distinguish between ⟨100⟩ directions parallel and perpendicular to its axis of alignment. A calculation of the energy level structure of $\mathbf{I}^0$ predicted that the $^3A_2$ state is 0.55 eV above a $^1B_1$ state, so this suggests that its EPR should not be observable.[9] This calculation suggested that $\mathbf{I}^0$ was susceptible to a scissorlike distortion, with its two p_π orbitals rotated in opposite directions about [100], lowering the symmetry to D_2. A more recent unpublished calculation has shown that the $^3A_2$ state is much closer to the $^1B_1$ state than 0.55 eV.[20]

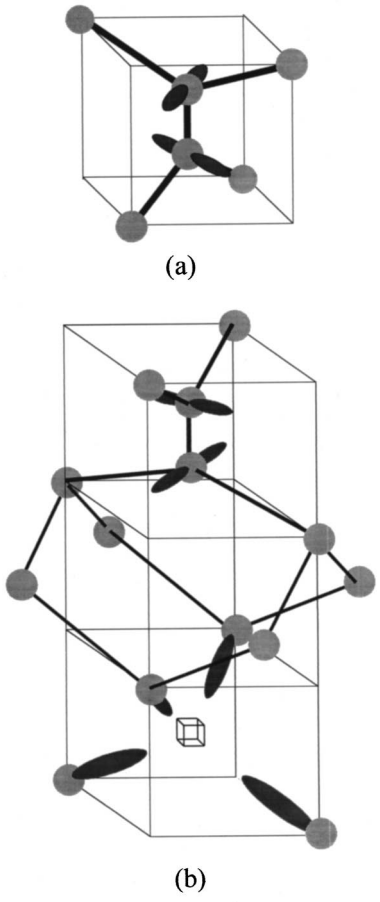

FIG. 1. The structure of (a) the ⟨100⟩-split interstitial, and (b) the ⟨100⟩-split interstitial compressed vacancy model [*I*-*V*] previously proposed for R2.

The theory[9] gave an upper bound for the migration energy of $\mathbf{I}^0$ as 1.7 eV, corresponding to migration around 500 K. In contrast, the formation of EPR defects by electron irradiation at 17 K, which change on subsequent annealing to 80 K, has been taken as evidence that **I** is mobile below 80 K.[21–23] Lea-Wilson and Lomer[24] cite a number of authors giving evidence for mobility of **I** at low temperatures. That $[\mathbf{I}-\mathbf{I}]^0$ [R1 (Ref. 3)] is formed by irradiation at 300 K indicates that **I** is mobile at this temperature, at least under the conditions of the irradiation, as it is improbable that $[\mathbf{I}-\mathbf{I}]^0$ would be formed directly by electron impact.

C. Previous work on R2

The EPR center R2 was described in 1962,[11] then labeled the *c* system. It is unlike most other radiation damage centers

in diamond in having very wide EPR lines and axial symmetry about ⟨100⟩. It was described by the spin Hamiltonian

$$\mathcal{H}=g\mu_B\mathbf{B}\cdot\mathbf{S}+D[S_z^2-\tfrac{1}{3}S(S+1)], \quad (1)$$

with $S=1$, $g=2.00$, and $D/h=4140$ MHz.[11] In subsequent work on electron and neutron irradiation, of any diamonds at any temperature, this center has always been reported. It has been unclear whether its concentration shows saturation as a function of irradiation dose, or whether the defect is intrinsic, or related to impurities. The many references to the EPR spectrum of this defect are listed in the catalog by Ammerlaan.[25]

Owen[26] showed, by measurements at 80, 200, and 295 K, that R2 corresponds to an excited state at 39 meV above the ground state. Owen further showed that the linewidth is independent of irradiation dose and of the temperature at which EPR is measured, and that it corresponded to a spread in the effective value of D.[26] He also found narrow lines for the $\Delta M_S=2$ transitions, because their width is affected only in second order by the value of D. He pointed out that such an abundantly created defect must have a simple structure, and prophetically expressed the opinion ''that the C_0 (carbon interstitial) identification . . . is to be preferred.''

The narrow $\Delta M_S=2$ transitions were studied by Nadolinny, Sobolev, and Yurieva[27] in an electron irradiated natural type-IIa diamond with a relatively low dislocation density, for which the typical linewidth of most EPR defects, like that of R1 or V^-, was 20 μT. For external field **B** exactly along ⟨100⟩, parallel to the axis of the defect, the intensity of the $\Delta M_S=2$ transition was zero. As **B** was rotated away from ⟨100⟩ the lines gained intensity, but also increased rapidly in width. For **B** between 1° and 1.5° from ⟨100⟩, a linewidth of about 20 μT allowed the resolution of ^{13}C hyperfine structure (hfs) from three sets of equivalent carbon neighbors that appeared to contain 8, 8, and 12 atoms, respectively, and with hyperfine splittings 0.71, 0.26, and 0.10 mT, respectively. For many defects in diamond, measurement of the angular variation of ^{13}C hfs lines due to neighboring ^{13}C nuclei ($I=\frac{1}{2}$), has been the vital information which has indicated the positions of the carbon atoms neighboring the defect (see Sec. V E). Unfortunately, the rapid increase in linewidth of the $\Delta M_S=2$ transitions for **B** in directions other than very close to ⟨100⟩, and the width of the $\Delta M_S=1$ transitions, precluded the use of this technique for characterizing R2.

The R2 defect appears to be remarkably stable at room temperature. It was still present in a neutron irradiated diamond more than 20 years after the irradiation.[28] In another investigation, the intensity of the R2 EPR signal was found to have increased in an electron irradiated sample after storage for several months.[23]

Walker[14] found two weak absorption lines in the optical spectrum of electron irradiated diamond at 1685 and 1859 meV, which correlated in intensity with the R2 EPR defect, and also annealed out at the same temperature, 700 K. The former line is very close to the much stronger zero-phonon line at 1673 meV of GR1, due to the neutral vacancy. The intensity of the 1685 meV line decreases with temperature below 80 K as though it originates from a level at 6(2) meV above the ground state which was thermally depopulated. Walker reported that the intensity of the line at 1859 meV appeared to increase in intensity below 80 K, by about 50% at 4 K, though it is not clear whether the evident sharpening of the line at 4 K was taken into account (see Sec. IV G).

A model of the defect was proposed to explain these optical spectra comprising a neutral vacancy displaced by a_0 along ⟨100⟩ from a neutral split interstitial aligned along ⟨100⟩.[29] In this model [Fig. 1(b)] $\mathbf{I}^0$ functioned as an internal source of stress to compress the vacancy along ⟨100⟩. It was proposed that the EPR observed was from the $^3B_1$ state of the compressed vacancy, which derives from the $^3T_1$ state of the uncompressed vacancy V^0. In the uncompressed state the $^3T_1$ state was assumed to be positioned at about 200 meV above the ground state. The compression, with axial stress estimated as 5.5 GPa, both lowers the energy of $^3B_1$ to the observed 39 meV, and produces a splitting of about 10 meV between the $^1A_1$ and lower $^1B_1$ components derived from the ^1E ground state of the uncompressed V^0. The optical line at 1685 meV is identified with the transition between $^1A_1$ and the excited $^1B_2$ state, corresponding to the experimental evidence for a lower state 6(2) meV above the ground state. We will label this model the *compressed vacancy model*. The $\mathbf{I}^0$ component was taken to be in its $S=0$ state.

III. EXPERIMENTAL DETAILS

A. Samples

Six high-temperature and -pressure (HTP) grown synthetic diamond samples were prepared with parallel polished faces of dimensions $\sim 2\times 2$ mm^2 and thickness ranging from 0.30 to 0.60 mm. Infrared and UV/visible absorption measurements prior to irradiation showed the samples to be type IIa. EPR measurements determined that the concentration of neutral single substitutional nitrogen N_s^0 [P1 (Ref. 25)] was less than 0.01 parts per million (ppm) carbon atoms, and infrared absorption measurements showed that the neutral boron concentration was less than 0.1 ppm.

Some of the diamonds had been isotopically enriched to $\ll$0.002%, 5%, 9%, and 50% ^{13}C by the method described by Twitchen *et al.*[3] The concentration of ^{13}C in the samples was confirmed from the position and width of the diamond Raman line, using the published data for the dependence of these parameters on the isotopic composition.[30–32] The characteristic Raman spectrum was measured using a conventional photoluminescence spectrometer, with excitation by an argon-ion laser operating in the 488–514 nm region, capable of measuring linewidths of very much less than 1 cm^{-1}.

A single sector synthetic type-Ib diamond, containing about 300 ppm N_s^0, was used in a comparative linewidth study (Sec. IV C).

B. EPR measurements

The EPR measurements of the paramagnetic defects were made at room temperature using two spectrometers: a Bruker ER200D spectrometer equipped with an X-band (nominally 9.5 GHz) bridge (ER 041 XG) and Bruker TE_{104} cavity, and a Clarendon designed and built Q-band (nominally 35 GHz) spectrometer described previously.[3] In the X-band spectrometer the sample was mounted on the end of a two circle goniometer, to allow precise alignment of the sample with

the magnetic field. Concentration measurements were made by comparing doubly-integrated first derivative EPR absorption spectra with those of a well-calibrated reference sample—a single growth sector HTP synthetic Ib diamond. Since the samples used in this study were never thicker than 0.6 mm, and, for 2 MeV electrons irradiation damage is produced to distances of ~ 3 mm,[33] it is justifiably assumed that the damage production rate is uniform through the thickness of the sample.

C. Optical measurements

Optical absorption measurements in the visible and UV range were made with a Perkin-Elmer Lambda 19 spectrophotometer. The sample was mounted in an Oxford instruments liquid-nitrogen cryostat (DN1704) and held at 80 K. The infrared measurements were made at room temperature using a Perkin-Elmer 1710 infrared Fourier-transform spectrometer. The concentration of V^0 was determined by integrating over the zero phonon line (ZPL) of GR1 and using the calibration factor determined by Twitchen *et al.*,[12] which relates the integrated intensity of GR1 to the concentration of V^0.

D. Electron irradiation

The electron irradiations were performed at Reading University, U.K. using a Van de Graaff accelerator giving a beam cross section of 1 cm^2. The diamonds were irradiated with 2 MeV electrons to doses which ranged between 2×10^{17} e^- cm^{-2} and 4×10^{18} e^- cm^{-2}. For irradiating diamonds at low temperatures, a special cryostat was developed, which is described elsewhere.[34] The temperature close to the sample was monitored continuously during the irradiation. Irradiations were made at measured sample temperatures of 100 and 350 K, and samples were allowed to return to 300 K before they were taken to Oxford for EPR measurements at 300 K.

One sample was irradiated at 100 K to a dose of 7×10^{17} e^- cm^2, and transferred to the X-band cavity for measurement at 90 K, without the temperature of the sample rising above 110 K using the technique described by Robinson.[35] The sample was then annealed in stages at temperatures of 150, 200, 250, and 293 K. At each temperature the sample was held for 2 h before cooling to 90 K to allow EPR measurements to be taken and compared at the same temperature. During these annealing cycles the sample was not exposed to any light radiation.

E. Annealing under uniaxial stress

A cell for applying uniaxial stress was constructed in the Clarendon Laboratory. Pressure is generated using argon gas in a sealed space at the top of the cell, with the force transmitted to the sample through the piston and diamond anvils. For a 1 mm^2 sample, pressures up to 4 GPa were achievable. On either side of the sample, sheets of copper were placed to take up any uneven stresses that might be caused due to imperfections in the polished parallel faces of the diamond sample. The piston shaft was of such a length that, after the sample had been loaded, it could be inserted into a preheated furnace (Severn Furnaces Ltd., UK, model SC50/2.5/1600). The heat capacity of the pressure cell was large, and it took up to 2 h for the temperature at the sample to stabilize. Consequently, low anneal temperatures were chosen, such that the anneal times were greater than 10 h, and the time for stabilization could be neglected. After the anneal was finished, the furnace temperature was ramped down to room temperature and the cell allowed to cool, before the stress on the sample was removed. When comparing the effect of annealing on a sample which had not been stressed to one that had, exactly the same procedure was followed with the sample loaded in the stress cell, but without any applied stress. The temperature was monitored by a thermocouple positioned close to the sample.

IV. PRESENT MEASUREMENTS

A. Production rates of R2 on electron irradiation

A variety of synthetic type-IIa diamonds of high quality and purity have been irradiated with 2 MeV electrons, both at 350 and at 100 K. These samples showed no EPR defects before irradiation. In the irradiation, V^0 and R2 were always formed, together with several other EPR centers [R1, (Ref. 3) R3, (Ref. 36), R14 (Ref. 36), and O3 (Ref. 34)]. In these samples EPR and optical measurements showed that V^0 was always the dominant charge state of the vacancy produced; and a small amount of V^- was detected which had a maximum concentration of $\sim 1/50$ that of V^0. Figure 2(a) shows the production of V^0 as a function of irradiation dose. The points represented by circles correspond to the 350 K irradiation and squares the 100 K irradiation. The straight line is a constrained fit to the experimental points made to pass through the origin. The measured production rate at both temperatures was $1.53(10)V^0$ cm^{-1} for 2 MeV electrons (Table I). Figure 2(b) shows the production of R2 in samples irradiated at 100 K (squares) [$1.1(1)$ cm^{-1}] and 350 K (circles) [$0.01(5)$ cm^{-1}]. The measured EPR concentrations at 300 K have been corrected allowing that R2 arises from a thermally excited state (see Sec. IV B).

The results of irradiating a sample to a dose of 7×10^{17} e^- cm^{-2} at 100 K and transferring to the spectrometer cold (see Sec. III D for details), showed on annealing in steps to 300 K that there was no measurable change in the EPR intensity from R1 and R2. Thus the difference between irradiating at 100 K and at 350 K does not result from some annealing stage which occurred between these two temperatures.

When irradiating with 2 MeV electrons the three differently oriented sites of R2 are created with equal probability, regardless of the direction of irradiation; in particular, irradiating through a (100) face along [100] did not preferentially create R2 centers aligned along [100].

B. Temperature dependence of the R2 EPR spectrum

Owen's measurements[26] establishing that the EPR of R2 arises from an excited state were made at only three temperatures between 80 and 295 K. We have made a careful measurement of the EPR intensity as a function of temperature T between 100 and 420 K. To allow for temperature-dependent effects on the sensitivity of the spectrometer, and the Boltzman distribution within the triplet state, we have taken the

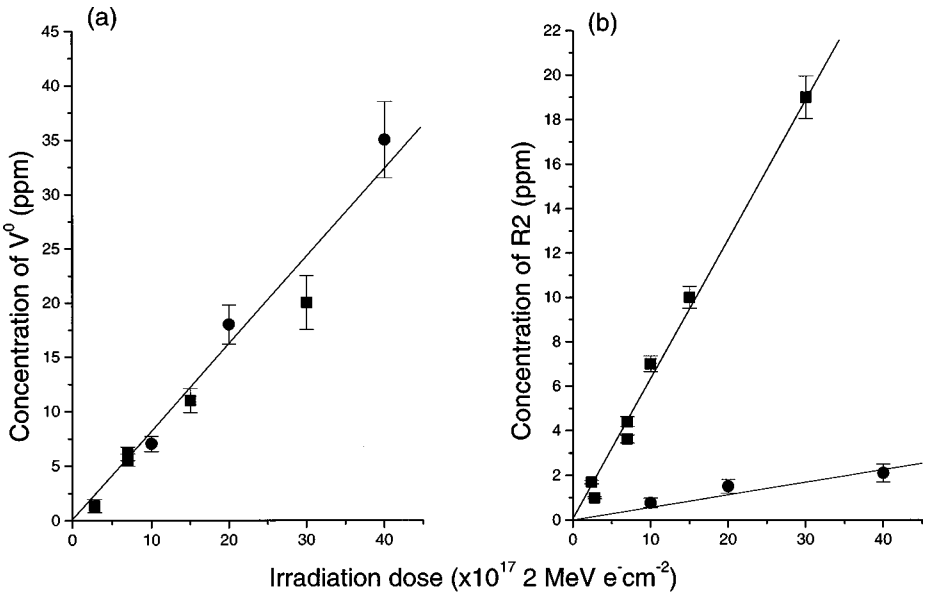

FIG. 2. (a) Concentration of neutral vacancies, as determined by the integrated absorption of the GR1 zero phonon line, produced in type-IIa diamond after irradiation with 2 MeV electrons. Circles represent vacancies created after irradiating at 350 K, and squares irradiating at 100 K, and then annealing to 300 K. The production rate of vacancies after both types of irradiation is the same: 1.53(10) cm^{-1}. (b) Production rate of the EPR defect R2. After irradiation with 2 MeV electrons at 100 K (squares) and 350 K (circles) the production rates are 1.10(10) cm^{-1} and 0.10(1) cm^{-1}, respectively.

ratio of the intensity of R2 to that of the EPR center R1, which is known to be in a ground triplet state.[3] The data are plotted in Fig. 3 and compared with a least-squares fit to a Boltzmann distribution over two energy levels of separation Δ, and with ratio g between the multiplicity of the lower to upper levels. So the fitted expression is

$$I(T)=I[1+g\exp(\Delta/k_BT)]^{-1}. \quad (2)$$

The illustrated curve in Fig. 3 corresponds to $\Delta=50(2)$ meV and $g=1/3$, assuming the levels to be orbital singlets, and the lower level to be a spin singlet and upper to be a spin triplet. In his fit, Owen took $g=2/9$, as he assumed that the upper state was $^3T_1$ and that the lower state a ^1E, corresponding to an uncompressed vacancy. For the compressed vacancy model, $g=2/3$, as the upper state is $^3B_1$ and there are two low-lying close singlets $^1A_1$ and $^1B_1$. The data may be fitted to these other values of g, leading to slightly different values of Δ, so these data do not allow any discrimination between these models of the energy level structure.

TABLE I. The production rates (cm^{-1}) in type-IIa diamond for 2 MeV electrons for the sample irradiated at 100 K compared with irradiation at a sample temperature of 350 K. The V^0 concentration was determined from the integrated intensity of the GR1 optical absorption zero phonon line. The R2 concentration was determined by EPR.

Temp. of irradiation (K)	V^0 (cm^{-1})	R2 (cm^{-1})
100	1.53(10)	1.10(10)
350	1.53(10)	0.10(1)

Two consequences of this variation of $I(T)$ are that (a) it is not possible to observe the EPR of R2 below about 77 K because the intensity becomes too weak and (b) allowance needs to be made for the thermal depopulation of the triplet state when estimating the concentration of the R2 defect from the integrated intensity of the EPR spectrum at 300 K. This increases the apparent concentration measured at 300 K by approximately a factor of 3.

C. Measurement of EPR linewidth variation

In an attempt to understand the origin of the EPR linewidth, measurements have been made on the six observed

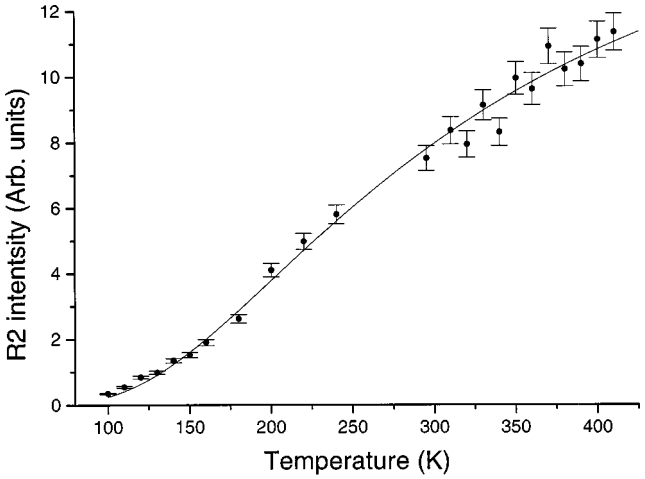

FIG. 3. Temperature variation of the peak-peak height of the first-derivative EPR spectrum of R2, normalized by dividing it by the peak-peak height of the first-derivative EPR spectrum of R1. The solid line corresponds to the best fit to Eq. (2), corresponding to $\Delta=50(2)$ meV.

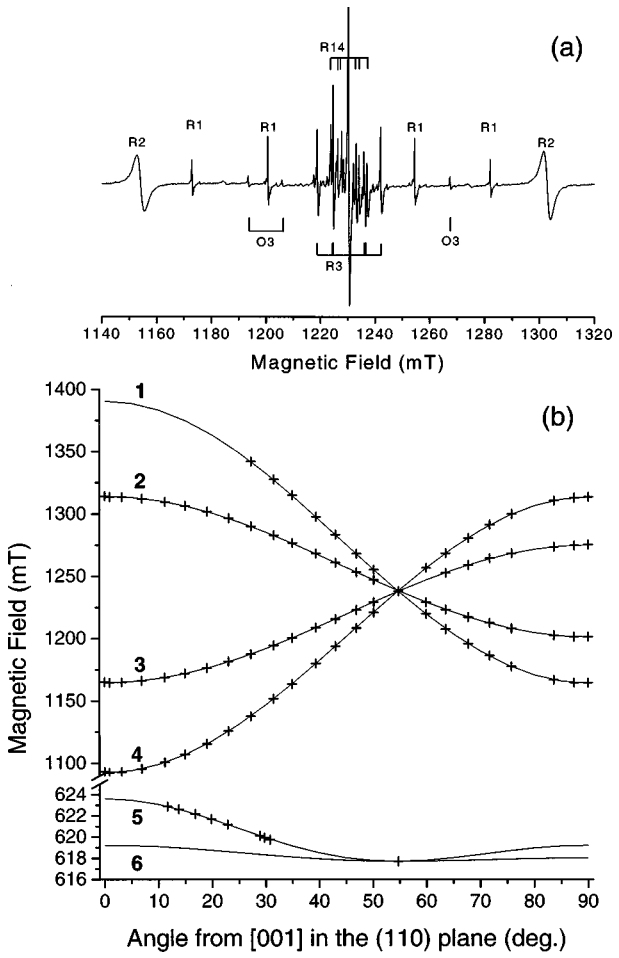

FIG. 4. (a) First-derivative EPR spectrum taken at 300 K with the Zeeman field oriented along a $\langle 001 \rangle$ crystallographic axis. The synthetic type-IIa sample had received a dose of 7×10^{17} (2 MeV e^-) cm^{-2} at 100 K. The dominant EPR defects are labeled. The absorption from R2 has *not* been multiplied by 3 to allow for the fact its arises from a thermally excited triplet state 50 meV above the singlet ground state. The outer pair of R2 lines lie outside the field range shown. Microwave frequency $\sim$35 GHz, microwave power $\sim$0.1 mW. (b) The angular variation of the EPR transitions from R2 centers for rotation of the magnetic field **B** about a $[1\bar{1}0]$ axis, with θ measured from [100]. The crosses are experimental line positions measured at frequencies of around 35 GHz. The solid curves are calculated using the **g** and **D** parameters determined from fitting the experimental data. Lines 1–4 correspond to $\Delta M_S = 1$ transitions, and 5 and 6 to $\Delta M_S = 2$ transitions.

lines, two *allowed* $\Delta M_S = 1$, and one *forbidden* $\Delta M_S = 2$ transitions for the two differently oriented defects in a $\{110\}$ plane. Measurements were made at both 9.6 and 35 GHz. A typical EPR spectrum with the Zeeman field oriented along a $\langle 100 \rangle$-crystallographic axis taken at the Q band is shown in Fig. 4(a). The sample had been irradiated to a dose of $7 \times 10^{17}\ e^-\ cm^{-2}$ at 100 K. Figure 4(b) shows the angular variation of the position of the six lines, and Figs. 5 and 6 show the previously unreported variation in their linewidth. The intensities of the $\Delta M_S = 1$ transitions do not show significant angular variation, but $\Delta M_S = 2$ transitions have zero intensity for **B** along the principal axis of the defect, say [100], and the fitted experimental intensity varies with the angle θ between **B** and this axis as $\alpha \sin^2\theta \cos^2\theta + \beta \sin^4\theta$.[37]

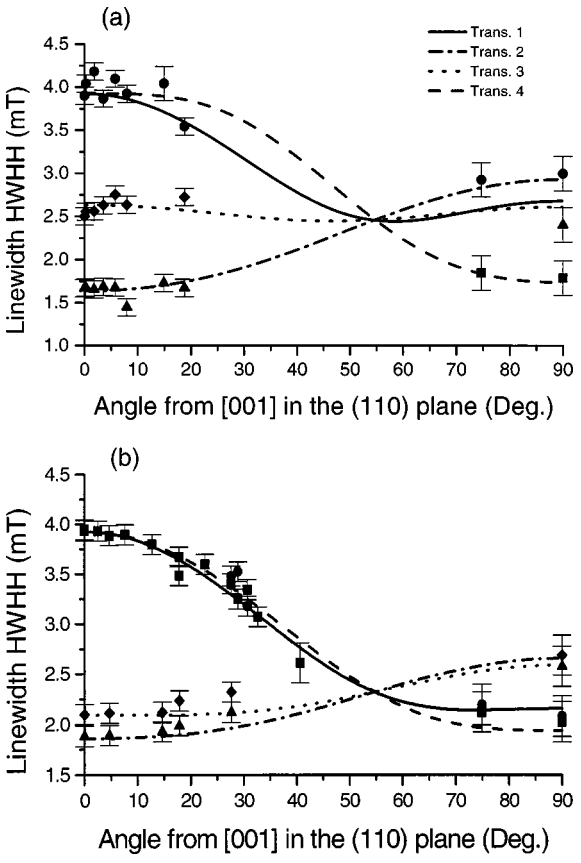

FIG. 5. The angular variation of the Lorentzian linewidths for the $\Delta M_S = 1$ transitions of R2 at (a) the X band and (b) the Q band. The line corresponds to the best fit of the data (symbols) to Eq. (5), which corresponds to the parameters $\delta D/h = 110(5)$ MHz and $\delta\theta = 0.6(1)°$.

The linewidths measured for **B** parallel to $\langle 100 \rangle$ and $\langle 110 \rangle$ are tabulated for various samples in Table II, including the much wider lines found in the type-Ib sample described in Sec. III A. Measurements showed that the EPR linewidths were independent of temperature between 70 and 650 K.

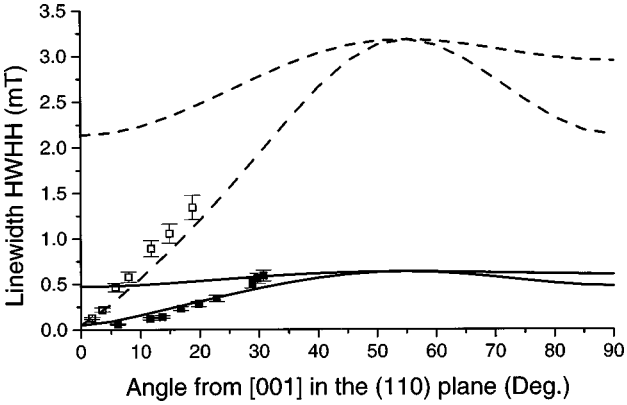

FIG. 6. The angular variation of the linewidths for the $\Delta M_S = 2$ transitions of R2 at the X band (dashed lines) and the Q band (solid lines). The lines correspond to the best fit of all the data to Eq. (5), which corresponds to the parameters $\delta D/h = 110(5)$ MHz and $\delta\theta = 0.6(1)°$.

TABLE II. The half-width at half-height linewidths (mT) of the EPR transitions labeled 1–6 in Fig. 2. (The error on linewidths is ~5%.)

^{13}C	**B**	Frequency	1	2	3	4	5,6
50	[100]	Q band	4.07	4.07	4.07		
50	[100]	X band	4.24	3.68	4.33	4.43	1.73
10	[100]	Q band	3.98	2.18	2.36		
10	[100]	X band		2.02	2.72	3.96	0.17
1	[100]	Q band	3.95	1.88	2.10		
1	[100]	X band		1.67	2.50	3.98	0.02
0.01	[100]	Q band	3.92	1.85	2.10		0.02
0.01	[100]	X band	3.92	1.64	2.63	3.92	
50	[011]	Q band	4.27	4.07			
0.01	[011]	Q band	1.94	2.64	2.57	2.13	
0.01	[011]	X band	2.68	2.94	2.62	1.74	
Type Ib	[100]	X band	5.00	3.44	2.21	4.65	

D. Measurement of the g and the D matrices

Equation (1) is a restricted form of the general spin Hamiltonian

$$\mathcal{H}=\mu_B \mathbf{S}\cdot\underline{\mathbf{g}}\cdot\mathbf{B}+\mathbf{S}\cdot\underline{\mathbf{D}}\cdot\mathbf{S} \tag{3}$$

for a paramagnetic defect with $S=1$ appropriate to axial symmetry and isotropic g value.

Figure 4(b) shows experimental data (crosses) taken at the Q band (nominally 35 GHz), which allows a better determination of the **g** matrix than at the X band, and fit to the spin Hamiltonian (solid lines). It is difficult to measure g values from the $\Delta M_S=1$ transitions, because of the large linewidth. However, the narrow EPR $\Delta M_S=2$ lines for **B** close to [100] give accurate values for $g_\parallel$. The best fit to Eq. (2) corresponded to an axial **g** matrix, where $g_\parallel=2.0021(1)$ and $g_\perp=2.0019(2)$, and an axially symmetric **D** matrix corresponding to $D/h(=\frac{3}{2}D_\parallel/h=-3D_\perp/h)=\pm 4173(3)$ MHz (measured at 300 K).

Measurements between 80 and 650 K showed that the magnitude of D decreased linearly with increasing temperature [$0.030(6)$ MHz K^{-1}]. This result is at odds with that reported by Kim and Choh.[28]

E. Measurement of ^{13}C hyperfine structure

The previous measurements of ^{13}C hyperfine structure (hfs) for **B** close to [100] were made on natural diamonds with 1.1% abundance of ^{13}C.[27] We have made similar measurements on diamonds isotopically enriched with 5% and 9% abundance ^{13}C, in an attempt to search for other hyperfine lines which might have been too weak for detection in the previous measurements. The larger concentration of ^{13}C leads to a proportional increase in the linewidth (~0.1–0.2 mT) due to electron-nuclear dipolar broadening. This allows only one pair of hyperfine satellites to be clearly resolved, and a second pair gives rise to unresolved wings to the central line. The intensity of this outer set of lines confirms the earlier finding that there are 8(1) equivalent sites for this set. Figure 7 shows a reconstruction using the parameters measured in Ref. 27. Significantly, no other hyperfine satellites have been detected further away from the center of the spectrum.

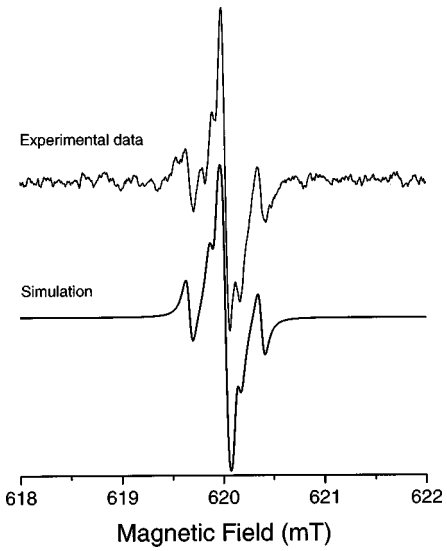

FIG. 7. The ^{13}C hyperfine structure on the $\Delta M_S=2$ transition for **B** near [100] at the Q band for a sample containing 5% ^{13}C, compared with a simulation assuming the ^{13}C hyperfine parameters corresponding to sets 8, 8, and 12 equivalent near neighbors with hyperfine splittings 0.71, 0.26, and 0.1 mT, respectively. See text for further details.

In a sample enriched with 50% ^{13}C, the R2 EPR lines were considerably wider than for samples with lower ^{13}C abundance and no additional structure was resolved. The EPR linewidths measured in this sample are also given in Table II.

F. Thermally induced reorientation of R2

Measurements were performed on a sample with polished parallel {100} faces, which was subjected to a uniaxial stress of 0.6 GPa during an anneal at 520 K for 10 h, i.e., at a temperature just at the beginning of the R2 annealing process. This was done to determine if there is any reorientation of the R2 centers away from the stress or alternatively preferential annealing of centers oriented parallel to the stress. After the anneal, the concentration of the site oriented with its principal axis parallel to the stress was found to have decreased by about 30%, while the concentration of the other two sites had each increased by about 15% (see Table III). This indicates reorientation without any overall loss of R2

TABLE III. The R2 concentration and ratio of intensities of transitions for defects aligned parallel ($d_\parallel$) to a uniaxial stress of 0.6 GPa applied at 520 K to the defects aligned perpendicular to the stress ($d_\perp$), compared with a sample annealed under the same conditions without stress.

Conditions	R2 concentration	Ratio of intensities of $d_\parallel:d_\perp$
Before stress	7.1(7) ppm	1.9(2)
After 0.6 GPa for 10 h	6.9(7) ppm	3.0(2)
After 0.0 GPa for 10 h	6.7(7) ppm	2.1(2)

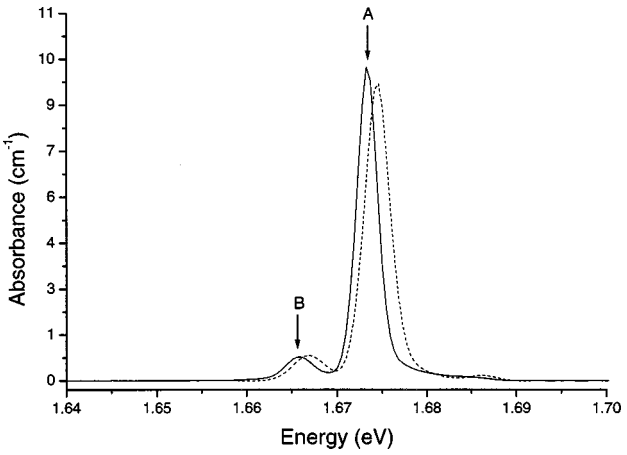

FIG. 8. The GR1 zero-phonon line absorption measured at ~80 K for a sample irradiated at 100 K to a dose of 3×10^{17} e^- cm^{-2}. The line labeled A arises from a $^1E_1$-$^1T_2$ transition, and B from ^1A-$^1T_2$. The dashed line shows the measured ZPL for the sample after irradiating at 100 K and annealing to room temperature. The solid line is the spectrum after the sample had been annealed at 750 K for 10 h.

centers. The sample was then annealed again at the same temperature, for the same duration, but without the applied stress. The concentrations of the three sites returned to their initial values to within the error bars, indicating the loss of the preferential orientation previously created using stress.

G. Optical properties

In Fig. 8 the broken curve measured at 80 K shows the $^1E_1$-$^1T_2$ and ^1A-$^1T_2$ transitions of V^0 (GR1) labeled A and B, respectively.[15,38] The sample was irradiated at 100 K to a dose of 2×10^{17} e^- cm^{-2} and annealed to 300 K. The V^0 concentration was 1.40(5) ppm. The solid curve shows the spectrum taken under the same conditions after the sample had been annealed at 750 K for 10 h. Following the anneal, the V^0 concentration was 1.00(5) ppm, and both transitions narrowed from 2.9(2) to 2.1(2) meV and shifted to lower energy by 1.0(2) meV.

The shape and position of spectra recorded for samples irradiated at 350 K are identical to the spectrum of this sample after the 10 h anneal (solid line). On careful inspection of the difference of the two spectra shown, we find that, although there is an overall decrease in the concentration of V^0, one part of the GR1 line on the low-energy side increases in intensity. After annealing at 750 K, the R2 (initial concentration 1 ppm) EPR defect had completely annealed out.

Figure 9 shows the relationship between the intensities of the weak lines at 1685 meV and 1859 meV: this is consistent with the earlier results.[14] We have also determined the constant of proportionality relating the integrated absorption of the line at 1859 meV to the concentration of R2 defects as $1.1(2)\times10^{-17}$ meV cm^{-2}. Between 90 and 4 K the 1.859 eV line sharpens up such that its measured peak height increases. A third optical line, at 3990 meV (R11), has recently been shown to have similar annealing characteristics to the 1859 meV line.[1,39] The correlation between these two lines for one particular sample on annealing is shown in Fig. 9(c).

When R2 anneals out, the concentration of V^0 decreases. In a sample irradiated with 2 MeV electrons at 100 K to a dose of 7×10^{17} e^- cm^{-2}, the concentration of V^0 falls by 30(3)% from 1.4 to 1.0 ppm, while that of R2 falls from 1.0 ppm to zero. In a sample irradiated at a higher temperature and flux, the fall in concentration of V^0 is only 14(2)% from 1.4 to 1.2 ppm, while the smaller concentration of R2 falls from 0.45 ppm to zero.

V. DISCUSSION

A. Previous models of R2

The fact that R2 is produced in all diamonds by irradiation with electrons and neutrons at any temperature up to 300 K (nominal, so the real temperature may be as much as 500 K), and in particular in the diamonds which we have used with extremely high purity, makes it clear that R2 is an intrinsic defect.

That the production rate for R2 at 100 K is so high, 1.1 cm^{-1} per incident 2 MeV electron, and not much smaller

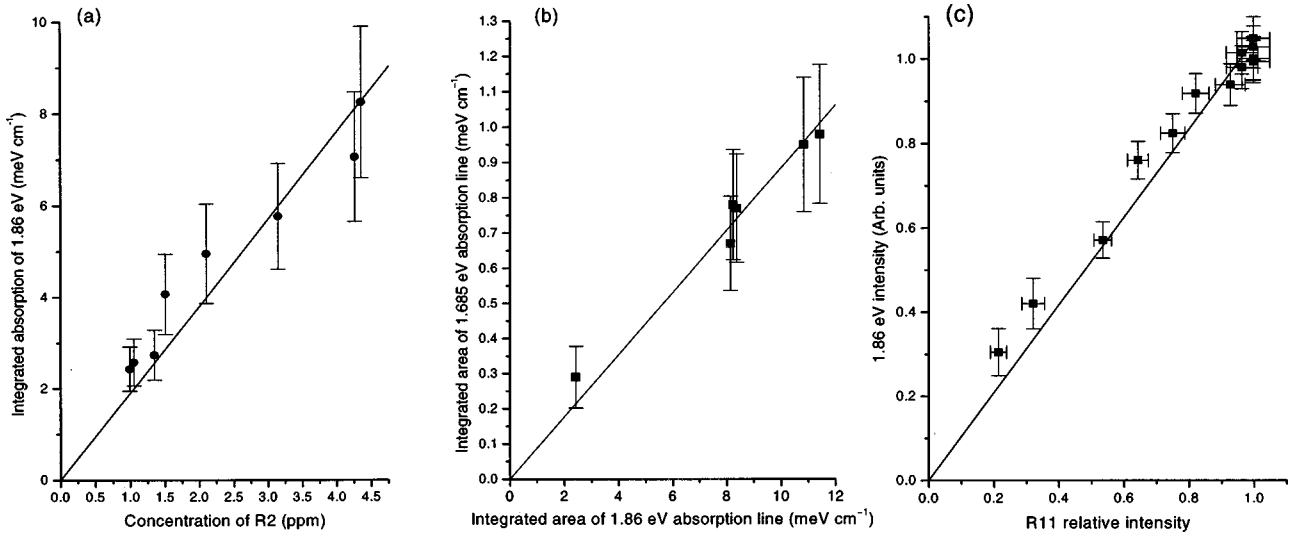

FIG. 9. The relationship between the integrated intensity of absorption of the three weak lines associated with R2 at (a) 1685 meV and (b) 1859 meV, and (c) the annealing out relationship between 1859 meV and 3990 meV (R11). See text for further details.

than the production rate for V^0, indicates that it must be a primary intrinsic defect with a simple structure.

Only two models have been proposed for defects satisfying these criteria, and with axial symmetry about ⟨100⟩: (a) the compressed vacancy model [*I*-*V*] described in Sec. II A [Fig. 1(b)]; (b) the isolated ⟨100⟩-split interstitial, $\mathbf{I}^0$ [Fig. 1(a)]. Strictly, model (a) with C_{2v} symmetry is not axially symmetric about [100], whereas model (b), with D_{2d} symmetry, is. A uniaxial stress on V^0 along [100] would produce D_{2d} symmetry, but the stress produced by a pointlike $\mathbf{I}^0$ is not uniaxial. That is not necessarily a serious objection on its own, as the deviation produced by $\mathbf{I}^0$ may be small.

For model (a), the EPR derives from an $S=1$ state on the vacancy, and one must suppose that the $S=1$ state of the $\mathbf{I}^0$ component is at too high an energy to be populated (in agreement with the theory of Breuer and Briddon[9]). For model (b) one must suppose that the latter theory is incorrect (consistent with the latest calculations[20]), and that the $S=1$ state of $\mathbf{I}^0$ lies at 50 meV above the ground state.

Furthermore, for model (b) one must suppose that $\mathbf{I}^0$ is not reorientating, or its EPR spectrum would be averaged out. For model (a), it would still be possible for isolated $\mathbf{I}^0$ to be mobile, while only those $\mathbf{I}^0$ associated with the compressed vacancy configuration were somehow stabilized.

A further consideration is that it is difficult to understand how the unique [*I*-*V*] configuration would be created. The chance of it occurring by direct impact is small, the carbon atom being knocked precisely along [100] into its new position. If this were to happen at all, it would probably be only at electron energies near the threshold for $\mathbf{I}^0$ production.

Certainly our experimental results show that impact of 2 MeV electrons directed along [100] does not preferentially create $\mathbf{I}^0$ with this orientation. For the compressed vacancy model to be correct, the interstitial must end up in that configuration after recoil.

B. Optical data

In the light of our determinations of the concentrations of R2 and V^0 in the diamonds we have studied (Sec. IV A and Table I), the compressed vacancy model is inconsistent with the very optical data it was invented to explain. Figure 8 shows the optical spectra of a diamond with concentrations 1.4 ppm of V^0 and 1.0 ppm of R2. In this model the weak line at 1685 meV due to R2 is the same line as GR1 of V^0 at 1673 meV, but shifted by the internal strain set up by the **I**, yet the ratio of intensities of the two lines is $\sim 30{:}1$, and the ratio of the concentrations of V^0 to R2 is only $\sim 3{:}2$. The measurements of the effect of uniaxial stress on the GR1 spectrum[16] did not show any marked change in the oscillator strength of the transition in the stress range needed to shift the line by 12 meV. Even allowing for the fact that the GR1 line is split into three by the strain, the measured ratios are completely inconsistent with the compressed vacancy model.

C. The $\underline{D}$ matrix

That $S=1$ indicates that two unpaired electrons are responsible for the EPR. For the compressed vacancy, these are orbitals of the vacancy; for $\mathbf{I}^0$, they are the p_π orbitals on the two principal C atoms.

D can arise from three mechanisms: (1) Interaction with the local environment through the mechanism of spin-orbit coupling $\lambda_{s.o.}\mathbf{L}\cdot\mathbf{S}$ where the $\lambda_{s.o.}$ is the spin-orbit coupling constant. (2) Magnetic spin-spin interaction between the two electrons. (3) Anisotropic exchange.

To first order, the orbital angular momentum of the electrons is quenched in the covalently bonded orbitals. However, spin-orbit coupling has matrix elements between the different orbitals, and mixes a small fraction of orbital angular momentum. This is different for different M_S states, and so contributes to *D*. The same mechanism contributes to a shift of *g* value from the free spin value. For orbitals on the same nucleus, these mechanisms are related, so that $D=\frac{1}{2}\lambda_{s.o.}(g_\parallel-g_\perp)$. The algebra is not so simple for orbitals on different nuclei, but this relationship probably can be used to indicate the magnitudes of contributions from this mechanism. The measured anisotropy of **g** (<0.0005) suggests that for $\lambda_{s.o.}\sim 106$ MHz,[40] this contribution to *D* is less than 100 MHz, and so can be discounted. Anisotropic exchange is also likely to be small, as it is mediated via spin-orbit coupling.

The zero-field interaction has not been calculated for a distorted vacancy, but one can get an idea of its likely magnitude from two measured examples of EPR centers involving unpaired electrons in a vacancy. W15 $[\text{N-}V]^-$ has C_{3v} symmetry about ⟨111⟩, and $D/h=2874$ MHz.[25,41] W26 [N-*V*-N], known to correlate with the optical H3 (2.463 eV) absorption, has C_{2v} symmetry about ⟨100⟩ and $D/h=-3945$ MHz.[25,42] In these centers the unpaired electrons are in orbitals primarily located on C atoms, and the internal strain is produced by the N atoms.

For $\mathbf{I}^0$, the spin-spin interaction may be estimated by assuming that the magnetic moment of a fraction η^2 of the unpaired electron probability density of each $S=1/2$ constituent electron is located on one of the two principal C nuclei, separated by distance *R*.

The magnetic dipole-dipole interaction leads to $D=3\eta^4 g^2\mu_B^2/R^3$. For $\eta^2=1$, the experimental value of *D* for R2 is consistent with $R=0.28$ nm. This is rather larger than one would expect for $\mathbf{I}^0$, but *R* would be smaller for $\eta^2<1$.

A correct calculation would take account of the distribution of the spin density on the p_π orbitals. We have made a calculation which is a little more realistic by supposing that half of the unpaired spin probability density on each p_π orbital is centered a distance *X* away from the nucleus, on each side along the line of the p_π orbital. If we retain *R* as the equilibrium internuclear distance, this gives the following expression for *D*:

$$D=(3\eta^4 4g^2\mu_B^2/R^3)\left\{\frac{(R^2-X^2)R^3}{(R^2+2X^2)^{5/2}}\right\}. \tag{4}$$

Taking reasonable values $R\sim 0.15$ nm and $X\sim 0.06$ nm, the factor in curly brackets is 0.42. Then, fitting the measured value of *D* to this expression gives $\eta^2=0.61$, a value only a little smaller than that in R1 (0.7).

These considerations show that the value of *D* alone cannot be used to discriminate between the two models: the measured value could be consistent with either.

D. Explanation of linewidth

The linewidth of the R2 EPR transitions is far too great to be due to the electron-electron spin-spin interaction, and the narrow $\Delta M_S = 2$ lines for **B** close to $\langle 100 \rangle$ show that the broadening is not due to short relaxation times. There is no clear reason why either of the proposed models should not give narrow lines like other radiation damage centers [for example, R1 or W15 (Ref. 25)], so it appears that neither model is consistent with these data.

The angular variations of the linewidths (half-width at half-height) shown in Figs. 5 and 6 are found to be consistent with the spin Hamiltonian given in Eq. (3) with a distribution of values of the components of $\underline{\mathbf{D}}$ about the mean value. Several systematic relationships have been tried between the various components of $\delta\mathbf{D}$, characterizing the difference between Eq. (3) and Eq. (1), but only one has been found which fits the experimental data. This corresponds to a specific form of $\underline{\mathbf{D}}$ which retains axial symmetry about an axis which deviates from the mean $\langle 100 \rangle$ direction by polar angles (θ, ϕ), such that the magnitude of D has rms (root-mean-square) deviation about the mean value of $|D_0| = 4140$ MHz, $\delta\theta$ has a rms deviation about a mean value of zero, and ϕ is randomly distributed over 2π. So, Eq. (1) can be retained, on the understanding that D and the symmetry z axis of the defect have distributions about the mean.

The value B_{res} of magnetic field required for resonance may be calculated from Eq. (1) as a function of the value of D and the angle θ between the z axis and $\langle 100 \rangle$, so that the derivatives $(\delta B_{res}/\delta D)$ and $(\delta B_{res}/\delta\theta)$ may be calculated. Then, distribution of values δD of D and $\delta\theta$ of θ contributes a linewidth δB_{res} where

$$\langle \delta B_{res}^2 \rangle = (\delta B_{res}/\delta D)\langle \delta D^2 \rangle + (\delta B_{res}/\delta\theta)\langle \delta\theta^2 \rangle. \quad (5)$$

The lines in Figs. 5 and 6 show the best fit to this equation, corresponding to $\delta D/h = 110(5)$ MHz and $\delta\theta = 0.6(1)°$.

Such a distribution might be set up by random internal strains, which would imply that the observed line is a superposition of many sites with slightly different D and θ values. Alternatively, the line might be motionally averaged between two (or more) extreme values. A characteristic of a motionally averaged spectrum is that at low temperatures (T) the lines are narrow, corresponding to two (or more) equivalent sites. Then as T increases, the system hops between the equivalent sites, leading first to a broad averaged line, and then at sufficiently high T to a narrow line at the mean position. Unfortunately it is not possible to measure R2 below 77 K, but that there is no perceptible change of linewidth between 77 and 650 K suggests that the broadening is not motional.

A further indication that the broadening is not motional, but rather due to internal strain, is that the lines of R2 are nearly 40% broader in a type-Ib diamond containing about 300 ppm of nitrogen, for which the dilatation of the lattice around the nitrogen atoms would be expected to set up internal strains (Sec. IV C and Table II).

This strongly suggests some potent mechanism for producing random internal strains, and a much greater sensitivity of R2 to the strain than other paramagnetic centers in diamond. The compressed vacancy model is not dissimilar to $V^-(S = 3/2)$, where a narrow EPR line shows no susceptibility to local strain produced by other defects in the material. However $\mathbf{I}^0$ might be sensitive to local strain, in comparison with most other EPR centers in diamond, because although the sp^3 bonded structure of diamond is particularly rigid, the sp^2 bonds at either end of $\mathbf{I}^0$ [Fig. 1(a)] may be particularly susceptible to displacement out of the plane of their sp^2 orbitals. We will return to consider the details of this mechanism in Sec. VI A.

One other result from the analysis of these data is that the angular variation of linewidth was found not to fit a modified Eq. (1) with an additional rhombic term $\delta E(S_x^2 - S_y^2)$, choosing x and y to be along either $\langle 100 \rangle$ or $\langle 110 \rangle$, which may be significant as one might expect a term of this type for the C_{2v} symmetry of the compressed vacancy.

E. The ^{13}C hyperfine structure

The ^{13}C hfs is described by additional terms in the Hamiltonian which becomes

$$\mathcal{H} = g\mu_B \mathbf{B}\cdot\mathbf{S} + D[S_z^2 - \tfrac{1}{3}S(S+1)] + \sum_i \mathbf{S}\cdot\underline{\mathbf{A}}_i\cdot\mathbf{I}_i, \quad (6)$$

where the summation is over all neighboring sites. The hyperfine structure terms are often found to have axial symmetry, and in this case may be decomposed by writing

$$\mathbf{S}\cdot\underline{\mathbf{A}}_i\cdot I_i = A_{si}\mathbf{S}\cdot\mathbf{I}_i + A_{pi}(3S_zI_{zi} - \mathbf{S}\cdot\mathbf{I}_i), \quad (7)$$

where $A_{si} = \eta_i^2\alpha_i^2 A_s^0$, $A_{pi} = \eta_i^2\beta_i^2 A_p^0$, and η_i^2 is the total spin density on the ith carbon neighbor, of which α_i^2 is the fraction of the $2s$ electron and β_i^2 is the fraction of the $2p$ electron orbital ($\alpha_i^2 + \beta_i^2 = 1$), A_s^0 is the hyperfine parameter for a single unpaired $2s$ electron in carbon, and A_p^0 is the hyperfine parameter for a single unpaired $2p$ electron on carbon. The z direction specifies the direction of the p-like lobe of the orbital, and $\lambda_i^2 = \beta_i^2/\alpha_i^2$ is the s-p hybridization ratio, which gives information about bond angles.[43,44]

As measurements on R2 are possible only for **B** close to $\langle 100 \rangle$, we need consider only neighboring sites which would be equivalent for that direction. For $\mathbf{I}^0$ the number of such sites for the central atoms (in bold), and those in shells with increasing numbers of bonds linking them to the central atoms are **2**;4;8,4;8,4;8,4; . . . and for the compressed vacancy: **2**, **2**;4,4,2,2;4,4,2,2;4,4,2,2; . . . . All of these, except the central atoms are expected to approximate to sp^3 bonded orbitals.

Unfortunately, as hfs can be measured only for one direction, the s-p hybridization of the unpaired electrons cannot be measured. If we assume that the orbitals are sp^3, the hyperfine separation for **B** along $\langle 100 \rangle$ is dominated by A_s. Hence the density $\eta_i^2\alpha_i^2$ may be deduced for three sets of neighbors containing 8, 8, and 12 atoms. For sp^3 orbitals, the spin density $\eta_i^2\beta_i^2$ is three times $\eta_i^2\alpha_i^2$. This assumption gives a total spin density of $\sim 25\%$ in the observed orbitals. This strongly suggests that there is a large contribution from central, and possible first-neighbor orbitals which are for some reason not being observed.

Although the multiplicity of equivalent sites may be increased by accidental coincidences, the observed pattern is much more consistent with R2 being $\mathbf{I}^0$ rather than a com-

pressed *V*. Another feature which favors $\mathbf{I}^0$ is that as much as 25% of the spin density appears to be on distant atoms. This is similar to R1, which includes $\mathbf{I}^0$. In contrast, V^- has ~100% of its unpaired electron probability density on the central four atoms,[8] the divacancy (R4/W6) has 82% on the central six atoms (although these are not all equivalent),[45] and the $^5A_2$ excited state of V^0 has 75% on the central four atoms.[46]

For $\mathbf{I}^0$, one might not observe the hfs from the central two atoms for **B** along ⟨100⟩ because that direction is perpendicular to both p_π orbitals, which if they are like the p_π orbitals in R1, have very small $A_\perp$. That would still leave the four next nearest neighbors, which would be more like sp^3 bonded orbitals, and so might be expected to be observable. It is possible that these lines might be broadened by a distribution of hyperfine parameters through a similar broadening mechanism to the fine structure parameter *D*.

Although for $\mathbf{I}^0$ the central atoms might not be expected to contribute for **B** along ⟨100⟩, they would contribute for **B** in other directions. This is not observable for natural diamonds, or even in the diamonds enriched to 9% ^{13}C, because of the wide lines. Their contribution may be greater than the linewidth, but their relative intensity would be too small. However, for large ^{13}C concentration, the contribution to the linewidth from unresolved hfs exceeds the other broadening mechanism.

On the assumption that the sets of eight equivalent neighbors whose hfs was observed by Nadolinny, Sobolev, and Yurieva[27] correspond to sp^3 bonded orbitals, one can use the hfs parameters determined for **B** along ⟨100⟩ to calculate the contribution to the linewidth due to these neighbors for any concentration of ^{13}C. This turns out to have the same magnitude (1 mT) for all four directions in which the linewidths have been tabulated (Table II). A comparison of the linewidth calculated by convoluting this hfs contribution and the linewidth observed for a sample with little ^{13}C, with the linewidths measured in samples containing 50% ^{13}C, indicates that there are substantial additional contributions from other neighbors.

In the absence of resolved hyperfine lines from additional neighbors, one can make only generalizations. It is significant that the additional contributions for **B** along ⟨100⟩, to both $\Delta M_S = 1$ and $\Delta M_S = 2$ lines, is much smaller than for **B** in the other three directions. For *p* orbitals directed along ⟨111⟩ directions, whatever the *sp* hybridization, the contributions from orbitals directed along all ⟨111⟩ directions sum to give the same contribution in the four directions we have tabulated. The measured difference is an indication of large anisotropic *p*-electron contributions, with ⟨100⟩ as a unique direction. This is consistent with a $\mathbf{I}^0$-like structure rather than a compressed vacancy structure. All known centers involving vacancies have the lobes of their *p* orbitals directed close to ⟨111⟩, and have $A_s \gg A_p$. In contrast, the p_π orbitals of $\mathbf{I}^0$ lie normal to ⟨100⟩, and would be expected to have very small $A_\perp$: only centers involving p_π orbitals [R1, (Ref. 39), W21 (Ref. 25)] have $A_s \sim A_p$.

It is interesting to continue to analyze the linewidths on the assumption that the center is $\mathbf{I}^0$, and that the hfs observed by Nadolinny, Sobolev, and Yurieva[27] corresponds to 8 of the 12 next-nearest neighbors. Hence, to a rough approximation, the additional linewidth for **B** along ⟨100⟩ can be taken as a contribution from the four next-nearest neighbors. On the assumption that these are sp^3 bonded, A_s for these neighbors is about 43 MHz, corresponding to about 18% of the unpaired spin density on these four atoms. This compares with 21% in Si-L8. When allowance has been made for the contribution from these neighbors in other directions, the residue can be attributed to the two central p_π orbitals, with $A_\parallel \sim 175$ MHz, $A_\perp \sim 32$ MHz, which corresponds to about 93% of unpaired electron in these two orbitals. All of these numbers are extremely approximate, because of the uncertainties of deconvoluting the linewidth. The sets of two and four equivalent neighbors, suggested by this interpretation of the linewidth, would certainly lead to observable resolved lines in the samples with 5% and 9% ^{13}C, even if they were too weak to be observed in natural diamond. That they are not observed is strong evidence that the hfs parameters for these neighbors have a distribution of values, which would give broad lines, even for low ^{13}C concentrations. A possible mechanism for this broadening will be discussed in Sec. VI A. Such broadening would also reduce the too large spin densities, suggested by the above interpretation, as it makes contributions to the overall linewidth in the sample with 50% ^{13}C, so making smaller the values of the hfs parameters deduced from the linewidth. A similar broadening mechanism could be invoked to account for the absence of hfs for four of the next-nearest neighbors; and this contribution would further reduce the hfs parameters necessary to account for the widths observed. Hence, one can account for the linewidth measured in the 50% ^{13}C sample on the $\mathbf{I}^0$ model with reasonable spin densities on the atoms, but not on the compressed vacancy model.

F. Annealing under uniaxial stress

That annealing under stress along a unique ⟨100⟩ at temperatures where the concentration of R2 is just beginning to fall for very long annealing times, causes reorientation of R2, so that the concentration of R2 compressed parallel to its axis decreases, while the other orientations increase (Sec. IV F), suggests relative motion of the constituents of R2 (see Table III). The reorientation of $\mathbf{I}^0$ is exactly what one would expect as it begins to become mobile. It is a much less probable process that the $\mathbf{I}^0$ component of the compressed vacancy would move round to the appropriate position for a rotated [*I*-*V*] combination. This would involve five steps, if the $\mathbf{I}^0$ is allowed to trespass into a ''chair'' containing the vacancy without being captured by it; and many more steps if it is to avoid such chairs. It seems much more likely that [*I*-*V*] compressed along its length would annihilate by recombination, removing irreversibly some of the population. Even if one supposes that such an improbable reorientation process could be driven by applied external pressure on [*I*-*V*], there is no reason why the reverse process should occur when the system is subsequently annealed again in the same way, but without any externally applied stress. Then, surely for the compressed vacancy model, there is no pressure to change the [*I*-*V*] orientation at all. However, for the $\mathbf{I}^0$ model, if all that happens at that temperature is that $\mathbf{I}^0$

begins to reorient, it is natural to expect that any nonequilibrium distribution set up by annealing under stress, should return to random orientation over the three sites.

Hence, this measurement seems to clinch the tendency indicated by most of the other evidence, to suggest that the compressed vacancy model is untenable, and that the isolated $\mathbf{I}^0$ model must be preferred.

VI. THE MODEL FOR R2

The above discussion seems to indicate conclusively that the compressed vacancy model is not the correct explanation of R2. However, some of the data discussed do not at first sight seem consistent with the isolated $\mathbf{I}^0$ model either.

A model which removes all of the inconsistencies of the $\mathbf{I}^0$ model is a loose association of $\mathbf{I}^0$ and V at a range of separations. The observed EPR is taken to arise from the $S=1$ state of $\mathbf{I}^0$, and the random strains at the $\mathbf{I}^0$ site, set up by a vacancy at different distances and directions from the $\mathbf{I}^0$ could be responsible for the broad EPR lines. In turn, the random strain at a V^0 site, set up by the distribution of neighboring $\mathbf{I}^0$ could give rise to the broadening of the GR1 line to the high-energy side.

There may be some evidence, in centers formed by electron irradiation of type-Ib diamond which are different from those in type-IIa diamond, that vacancies may be formed preferentially near to N_s^0 atoms.[7] However, the density of N_s^0 is so low that in the major part of the volume of the diamond one would expect the probability of generation of R2 to be the same as in type-IIa, and that the major part of the observed intensity of the EPR attributable to R2 would come from this region. Hence, one should regard the additional broadening of R2 in type-Ib diamond as a bulk effect of the distribution of N_s^0 upon a random distribution of R2 centers. In contrast, the independence of the linewidth of R2 upon the concentration of R2 (and V^0) indicates that the strain which broadens its lines must be produced by locally formed vacancies.

Under normal conditions, $\mathbf{I}^0$ is immobile up to the annealing temperature. The data of Sec. IV G suggest that on annealing, some $\mathbf{I}^0$ recombine with their local V, so reducing the overall V concentration: about 40(6)% in the 100 K irradiated sample with high initial R2 content, and 50(6)% in the sample irradiated at 350 K. The others diffuse away to other fates. The remaining V^0 are no longer strained, so the GR1 lines become sharp.

The spin-packet width of the EPR line ($\sim 20\ \mu$T) is about two orders of magnitude smaller than the EPR linewidth, so there must be more than 100 different neighboring sites contributing to the broadening. There are ~ 250 sites for V^0 between radial distances a_0 and $2a_0$ from $\mathbf{I}^0$, so that this is not an unreasonable number.

This model suggests that R2 is formed by particle impact ejecting a carbon atom to an interstitial site a few bondlengths away. Any which do not get further than the 3rd- neighbor position, so are in the same chair, immediately recombine; but the others remain immobile at the site where the impact leaves them. For any site, $\mathbf{I}^0$ could be oriented along any of the three $\langle 100\rangle$ axes.

A. The line broadening mechanism

In Sec. V D, we suggested that $\mathbf{I}^0$ might be more sensitive to local strain than other EPR centers in diamond, because the sp^2 bonds on either end of $\mathbf{I}^0$ [Fig. 1(a)] may be particularly susceptible to displacement out of the plane of their sp^2 orbitals.

This can be modeled by displacing the two nuclei by a distance Y_1 and Y_2 along their respective p_π orbitals. To save cumbersome expressions, we calculate this on the assumption that η^2 of the spin density is concentrated on each nucleus, and calculate the dipole-dipole interaction between them (elaboration of this to take account of the distribution of spin density over the p_π orbitals gives essentially the same conclusion). Expressed in terms of D for the undisplaced nuclei, this leads to

$$\Delta D/D = 6(Y_1^2+Y_2^2)/R^2 = -3\Delta R/R, \tag{8}$$

$$\sin\theta = (Y_1^2+Y_2^2)^{1/2}/R, \tag{9}$$

$$\tan\phi = Y_1/Y_2. \tag{10}$$

That ϕ takes all values indicates that Y_1 and Y_2 are uncorrelated, with $\langle Y_1^2\rangle = \langle Y_2^2\rangle$ and $\langle Y_1\rangle = \langle Y_2\rangle = 0$. The distribution of values of D and θ about a mean gives the rms deviations of $\delta R/R$ and $\delta\theta = \langle (Y_1^2+Y_2^2)^{1/2}\rangle/R$. Taking $R \sim 0.15$ nm the experimentally observed $\delta D/D$ and $\delta\theta$ indicate values of $\delta R \sim 1.3\times 10^{-3}$ nm and $\langle (Y_1^2+Y_2^2)^{1/2}\rangle \sim 1.6\times 10^{-3}$ nm.

It does not seem unreasonable that this sort of magnitude of distortion could be produced by nearby vacancies. It is difficult to estimate the internal strain set up by particular defects. One can approximate by using the results of Anthony,[47] who showed that under certain approximations the internal stress set up by a sphere inserted in diamond would fall off as r^{-3} from the center, so one may assume that the strain would do likewise. For N_s^0 there is a $\sim 25\%$ expansion of the principal N_s^0-C bond, which is elongated to ~ 0.2 nm.[48–50] For 300 ppm of N_s^0 the mean distance from any carbon atom site (potential site for **I**) is 1.4 nm, at which distance therefore there would be a typical strain of 10^{-3}, which is the order of magnitude to produce the broadening we observe. For V^0 the nearest neighbors at 0.15 nm are displaced outwards by 15%,[8] so at distance a_0 (appropriate for the compressed vacancy model) the strain is $\sim 10^{-2}$, and it becomes $\sim 10^{-3}$ at ~ 0.8 nm ($2.2a_0$). This suggests that the V^0 which broaden the R2 line lie within $3a_0$ of $\mathbf{I}^0$. This also suggests that the contribution to the R2 line from any compressed vacancy site should be displaced by about 25 mT, but if the probability of such sites is only $\sim 3\%$ this would not be observable.

The displacement we have deduced above of the nuclei of the p_π orbitals might be expected to modify the spin density on them appreciably, and hence their hyperfine interaction. So the hfs parameters for the central atoms could suffer a random distortion like D. This would broaden the hyperfine lines, even in the $\Delta M_S = 2$ transitions, which are almost insensitive to D. The modulation of the sp^2 bonds of the central nuclei would also modify the sp^3 bonds on the four nearest neighbors, which might also therefore have signifi-

cant spread of hfs parameters. This may also produce the same sort of effect on the four second neighbors in the same {110} plane as the central atom and the nearest neighbor, which could account for there being only 8 of the 12 second neighbors with narrow hfs lines.

VII. CONCLUSION

The most abundant paramagnetic defect formed on electron irradiation of IIa diamond is R2. It is created in similar concentration to the vacancy at 100 K, but on irradiating at 350 K the production rate is a factor of 10 or more down. Present experimental data on creation rates, EPR linewidth, g value, hyperfine structure, optical absorption, and annealing under uniaxial stress have been combined with old data on hyperfine structure, fine structure parameter D, and optical data, to conclude that the EPR arises from an excited $S=1$ state, 50 meV above an $S=0$ ground state of the neutral carbon ⟨100⟩-split interstitial, $\mathbf{I}^0$, created in association with a nearby vacancy at any site more distant than a_0. $\mathbf{I}^0$ remains immobile until the annealing temperature of 700 K. Optical transitions at 1.685, 1859, and 3995 meV show a direct correlation in intensity with the R2 EPR concentration.

ACKNOWLEDGMENTS

This work was supported by the Engineering and Physical Sciences Research Council (EPSRC) Grant No. GR/L65772. D.J.T. thanks Merton College, Oxford, Linacre College, Oxford and EPSRC for financial support. D.C.H. thanks EPSRC and De Beers Industrial Diamond Division (UK) Ltd, for financial support. M.E.N. acknowledges EPSRC for financial support. We would also like to thank Ian Thomas for his invaluable help with the Reading van De Graaf accelerator and Mark Witney (Clarendon Laboratory) for construction of the irradiation dewar.

*Author to whom correspondence should be addressed. Present address: King's College, London, Strand, London WC2R 2LS, U.K.

[1] L. Allers, A. T. Collins, and J. Hiscock, Diamond Relat. Mater. **7**, 228 (1998).
[2] A. Mainwood and A. M. Stoneham, J. Phys.: Condens. Matter **9**, 2453 (1997).
[3] D. J. Twitchen, M. E. Newton, J. M. Baker, O. D. Tucker, T. R. Anthony, and W. F. Banholzer, Phys. Rev. B **54**, 6988 (1996).
[4] L. Allers, A. S. Howard, J. F. Hassard, and A. Mainwood, Diamond Relat. Mater. **6**, 353A (1997).
[5] A. Mainwood *et al.*, J. Phys. D **28**, 1279 (1995).
[6] J. W. Prins, Diamond Relat. Mater. **7**, 1065 (1998).
[7] G. Davies, S. C. Lawson, A. T. Collins, A. Mainwood, and S. J. Sharp, Phys. Rev. B **46**, 13 157 (1992).
[8] J. Isoya, H. Kanda, Y. Uchida, S. C. Lawson, S. Yamasaki, H. Itoh, and Y. Morita, Phys. Rev. B **45**, 1436 (1992).
[9] S. J. Breuer and P. R. Briddon, Phys. Rev. B **51**, 6984 (1995).
[10] A. Mainwood, F. P. Larkins, and A. M. Stoneham, Solid-State Electron. **21**, 1431 (1978).
[11] E. A. Faulkner and J. N. Lomer, Philos. Mag. **7**, 1995 (1962).
[12] D. J. Twitchen, D. C. Hunt, V. Smart, M. E. Newton, and J. M. Baker, Diamond Relat. Mater. **8**, 1572 (1999).
[13] C. D. Clark, R. W. Ditchburn, and H. B. Dyer, Proc. R. Soc. London, Ser. A **237**, 75 (1956).
[14] J. Walker, J. Phys. C **10**, 3867 (1977).
[15] C. D. Clark and J. Walker, Proc. R. Soc. London, Ser. A **334**, 241 (1973).
[16] G. Davies and C. M. Penchina, Proc. R. Soc. London, Ser. A **338**, 359 (1974).
[17] D. W. Palmer, Ph.D. thesis, University of Reading, 1961.
[18] L. Allers, A. T. Collins, and J. Hiscock, Diamond Relat. Mater. **7**, 228 (1998).
[19] D. J. Twitchen, D. C. Hunt, C. Wade, M. E. Newton, J. M. Baker, W. F. Banholzer, and T. R. Anthony, Physica B (to be published).
[20] J. Goss (private communication).
[21] J. N. Lomer and A. M. A. Wild, Philos. Mag. **24**, 273 (1971).
[22] J. N. Lomer and D. Marriott, Inst. Phys. Conf. Ser. **46**, 341 (1979).
[23] I. T. Flint and J. N. Lomer, Physica B & C **116B**, 183 (1983).
[24] M. A. Lea-Wilson and J. N. Lomer, Philos. Mag. A **74**, 685 (1996).
[25] C. A. J. Ammerlaan, in *Impurities and Defects in Group IV Elements and III-V Compounds*, edited by M. Schulz, Landolt-Bornstein, New Series Group III, Vol. 22(b) (Springer, Berlin, 1998), p. 205.
[26] J. Owen, in *Physical Properties of Diamond*, edited by B. Berman (Oxford University Press, Oxford, 1965), Chap. 10, p. 274.
[27] V. A. Nadolinny, E. V. Sobolev, and O. P. Yurieva, J. Struct. Chem. **626**, 36 (1995).
[28] J. S. Kim and S. H. Choh (private communication).
[29] A. Mainwood, J. E. Lowther, and J. A. wan Wyk, J. Phys.: Condens. Matter **5**, 7929 (1993).
[30] T. R. Anthony and W. F. Banholzer, Diamond Relat. Mater. **1**, 717 (1991).
[31] K. C. Hass, M. A. Tamor, T. R. Anthony, and W. F. Banholzer, Phys. Rev. B **44**, 12 046 (1991).
[32] R. M. Chrenko, J. Appl. Phys. **63**, 5873 (1988).
[33] C. D. Clark, P. W. Kenney, and E. W. J. Mitchell, Discuss. Faraday Soc. **31**, 96 (1961).
[34] D. J. Twitchen, D. C. Hunt, M. E. Newton, J. M. Baker, W. F. Banholzer, and T. R. Anthony, Physica B (to be published).
[35] P. T. Robinson, D. Phil. thesis, University of Oxford, 1985.
[36] M. A. Lea-Wilson, J. N. Lomer, and J. A. van Wyk, Philos. Mag. B **70**, 101 (1995).
[37] A. Abragam and B. Bleaney, *Electron Paramagnetic Resonance of Transition Ions* (Clarendon Press, Oxford, 1970), p. 159.
[38] C. A. Coulson and M. J. Kearsley, Proc. R. Soc. London, Ser. A **241**, 433 (1957).
[39] D. J. Twitchen (private communication).
[40] J. E. Lowther and J. A. van Wyk, Phys. Rev. B **49**, 11 010 (1994).
[41] J. H. N. Loubser and J. A. van Wyk, Diamond Research (Suppl. to Ind. Diamond. Rev.), 11 (1977).
[42] J. A. van Wyk and J. H. N. Loubser (private communication).
[43] G. D. Watkins and J. W. Corbett, Phys. Rev. **121**, 1001 (1961).
[44] J. R. Morton and K. F. Preston, J. Magn. Reson. **30**, 577 (1978).
[45] D. J. Twitchen, M. E. Newton, J. M. Baker, T. R. Anthony, and W. F. Banholzer, Phys. Rev. B **59**, 12 900 (1999).
[46] J. A. van Wyk, O. D. Tucker, M. E. Newton, J. M. Baker, G. S. Woods, and P. Spear, Phys. Rev. B **52**, 12 657 (1995).
[47] T. R. Anthony, Diamond Relat. Mater. **4**, 83 (1994).

[48] S. A. Kajihara, A. Antonelli, J. Bernholc, and R. Car, Phys. Rev. Lett. **66**, 2010 (1991).
[49] R. Jones, P. R. Briddon, and S. Oberg, Philos. Mag. Lett. **66**, 67 (1992).
[50] P. R. Briddon, M. I. Heggie, and R. Jones, in *Proceedings of the 2nd International Conference on New Diamond Science and Technology 1991*, edited by R. Messier, J. T. Glass, J. E. Butler, and R. Roy, MRS Soc. Symp. Int. Proc. NDST-C3 (Materials Research Society, Pittsburgh, 1991), p. 63.